Supporting Information

Tuning the electronic environment of the atoms coordinating $CuCl_x$ species to regulate vinyl chloride production

Qidi Liu[a], Yunsheng Dai[b], Dong Huang[d], Yongsheng Xu[a, *], Yanzhao Donga, Dongyang Xie[a], Jinli Zhang[a, c], Haiyang Zhang[a, *]

[a] *School of Chemistry and Chemical Engineering/State Key Laboratory Incubation Base for Green Processing of Chemical Engineering, Shihezi University, Shihezi 832000, China*

[b] *Yunnan Precious Metals Lab Co., Ltd., Kunming 650106, China*

[c] *School of Chemical Engineering and Technology, Tianjin University, Tianjin 300354, China*

[d] *Xinjiang Tianye Co., Ltd., Shihezi 832000, China*

Contents

Text S1. Evaluation and of catalysts.

The catalyst performance was evaluated in a fixed bed glass microreactor under normal pressure and 180 °C. First, N_2 is injected into the pipeline 30 minutes before the reaction starts to remove residual water and impurity gas. Subsequently, N_2 was switched to HCl gas, which was used to activate the catalyst (3 mL) in the reactor for 30 minutes. When the temperature in the reactor rises to 180 °C, C_2H_2 gas is passed into the reaction system, and the acetylene hydrochlorination reaction begins. The volume ratio of HCl to C_2H_2 (V_{HCl}/V_{C2H2}) is controlled at = 1.15, and the gas hourly space velocity (GHSV) of acetylene was controlled at 180 h^{-1}. The gaseous product was analyzed quantitatively by gas chromatography after impurity removal and drying. Finally, the performance of the catalyst was evaluated according to the calculated acetylene conversion and vinyl chloride selectivity.

Text S2. Characterization of catalysts.

Programmed Temperature Desorption (TPD) Measurements. The TPD tests were performed on an automated chemosorbent (Quantachrome, Chembet Pulsar TPR/TPD), scanned within the temperature range of 30 to 600 °C with a heating rate of 5 °C/min. For TPD experiments, the samples entirely adsorbed the corresponding gas prior to test.

X-ray Photoelectron Spectroscopy (XPS) Measurement. All spectra were performed on an energy spectrometer containing an Al-Kα X-ray source (Thermo Fisher, Escalab 250Xi). The relative data were processed on Advantage. The calibrated energy of C 1s was 248.8 eV.

Programmed Temperature Reduction (H_2-TPR) Measurements. The H_2-TPR tests were performed on an automated chemosorbent (Quantachrome, Chembet Pulsar TPR/TPD).

Accurately weigh 0.1 g of the sample and place it in a U-shaped quartz tube, with both ends filled with an appropriate amount of quartz wool. The flow rate of the 10% H_2/Ar mixed gas was maintained at 100 mL·min^{-1}. The temperature was increased from room temperature to 900 °C at a heating rate of 10 °C·min^{-1}, and TCD signals were recorded throughout this range. The position and area of the hydrogen consumption peak were analyzed to determine the valence state of the active metal species.

Scanning Transmission Electron Microscopy (STEM) Measurements. The separation of metal nanoparticles within the catalyst was examined using a transmission electron microscope (JEOL JEM-F200). Morphology and particle size were analyzed as follows: A small quantity of the sample was ground into powder and placed into a centrifuge tube. An ethanol solution was then added, and the mixture was placed in an ultrasonic bath for uniform dispersion. Subsequently, a small volume of the supernatant was dropped onto a 200/300 mesh grid. The grid was dried under infrared light and examined using the transmission electron microscope at an accelerating voltage of 200 kV.

X-ray Diffraction (XRD) Analysis. X-ray diffraction (XRD) analysis of the catalyst samples was conducted using a Bruker D8 ADVANCE X-ray diffractometer. The operating voltage and current were set at 40 kV and 40 mA, respectively, with a scanning speed of 10° per minute over the range of 2θ = 10-90°. Data collection aimed to analyze the variations in the crystal phase structure of metals present in the samples.

Thermogravimetric Analysis (TGA). Thermogravimetric experiments were carried out using a Netzsch STA 449 F5 thermal analyzer. Initially, approximately 10 mg of sample was

loaded. Subsequently, under an air atmosphere with a flow rate of 50 mL/min, the temperature was increased gradually from 25 °C to 900 °C at a heating rate of 10 °C/min. During this process, thermogravimetric (TG) and derivative thermogravimetric (DTG) data were collected to analyze the carbon content deposited on the catalyst surface during the reaction.

Fourier transform infrared spectroscopy (FT-IR). FT-IR analysis was performed on a Bruker Vertex70 FT-IR spectrophotometer. A small amount of the sample was ground and then tablets were pressed for scanning. The wavenumber range was set from 400 to 4000 cm^{-1}, and the information on the surface functional groups of the sample was obtained. *In-situ* diffuse reflection infrared Fourier transform spectroscopy (DRIFTS): The *in-situ* DRIFTS of catalysts was performed using a Bruker Vertex70 FT-IR spectrophotometer with a DTGS detector. The total gas flow was controlled at 5 mL/min. The volume ratio and temperature were controlled as same as the reaction conditions. The temperature was controlled at 180℃. The test spectrum was adjusted to 3000-3500 cm^{-1}.

Text S3. Density functional theory calculation.

The density functional theory (DFT) calculations were carried out with the Materials Studio (MS). The structural optimization adopts the Dmol3 module in Materials Studio, The Becke-Lee-Yang-Parr (BLYP) functional within generalized gradient approximation (GGA) was used to process the exchange-correlation, which was utilized to describe the expansion of the electronic eigenfunctions [1]. All atoms are fully relaxed until the force, displacement, energy, and difference are less than 0.002 Ha/Å, 0.005 Å, 10^{-5} Ha, respectively. Open the charge density preprocessing option and set the maximum value of Subspace Iterative Inverse (DIIS) to 6 to

significantly improve self-consistent field convergence. We analyze the electron transfer process through three distinct approaches: calculating the atomic charge numbers, determining the Hamiltonian population of the crystal orbitals, and examining the projected density of states.

The adsorption energy (E_{ads}) of a complex formed between two molecules, A and B, can be calculated using the following equation:

$$E_{ads} = E_{complex} - (E_A + E_B) \quad \text{(S1)}$$

where $E_{complex}$ is the total energy of the molecular complex of A and B. E_A is the energy of the ligand, E_B is the energy of hydrogen chloride or acetylene, respectively.

The formation energy (E_f) of copper clusters can be calculated by the following formula:

$$E_f = E_{Cluster} - (E_{Cu} * n_{Cu} + E_{Cl} * n_{Cl}) \quad \text{(S2)}$$

where $E_{Cluster}$ is the total energy of the copper cluster, E_{Cu} is the energy of the copper atom, and E_{Cl} is the energy of the chlorine atom. The n_{Cu} represents the number of copper atoms, and n_{Cl} represents the number of chlorine atoms

Text S4. Calculations of conversion, selectivity and deactivation rate.

Four indicators, including conversion, selectivity, deactivation rate [2], in this manuscript were used to evaluate the catalytic performances and the detailed calculations were as follows:

$$Conversion\ (\%) = \frac{C_{inlet} - C_{outlet}}{C_{inlet}} \times 100 \quad \text{(S3)}$$

$$Selectivity\ (\%) = \frac{C_{C2H3Cl}}{C_{inlet} - C_{outlet}} \times 100 \quad \text{(S4)}$$

$$Deactivation\ rate\ (h^{-1}) = \frac{Conversion_{max} - Conversion_{t}}{\Delta t_1} \quad \text{(S5)}$$

where C_{inlet} and C_{outlet} represent the concentration of C_2H_2 at the inlet and outlet of reactor, respectively. C_{C2H3Cl} is the concentration of C_2H_3Cl at the outlet of reactor, $\text{Conversion}_{\text{max}}$ is the maximum C_2H_2 conversion, $\text{Conversion}_{\text{t}}$ is the last C_2H_2 conversion in the experiment, and Δt_1 is the time taken for conversion to decrease from maximum to residual levels.

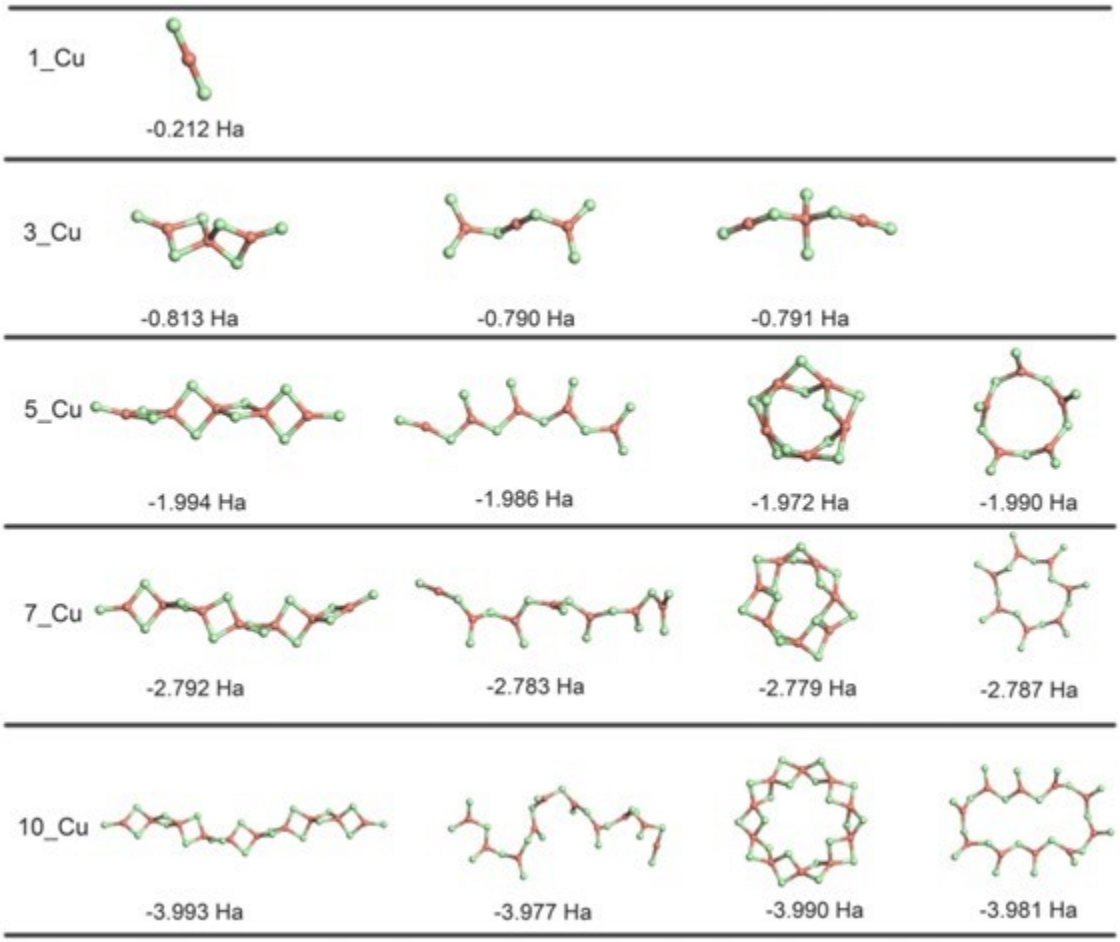

Figure S1. Different models of copper clusters. (The formation energy is listed beneath the corresponding structure)

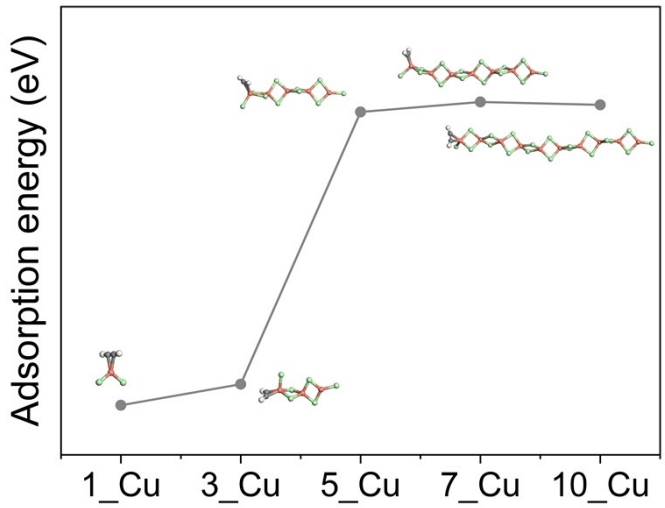

Figure S2. Adsorption energy of acetylene on the linear configuration of $CuCl_x$ model. (The insets are the relative optmized strucutre)

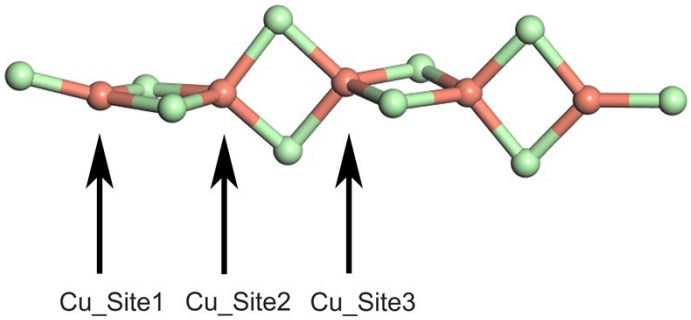

Figure S3. Classification of Cu sites in the optimized configuration.

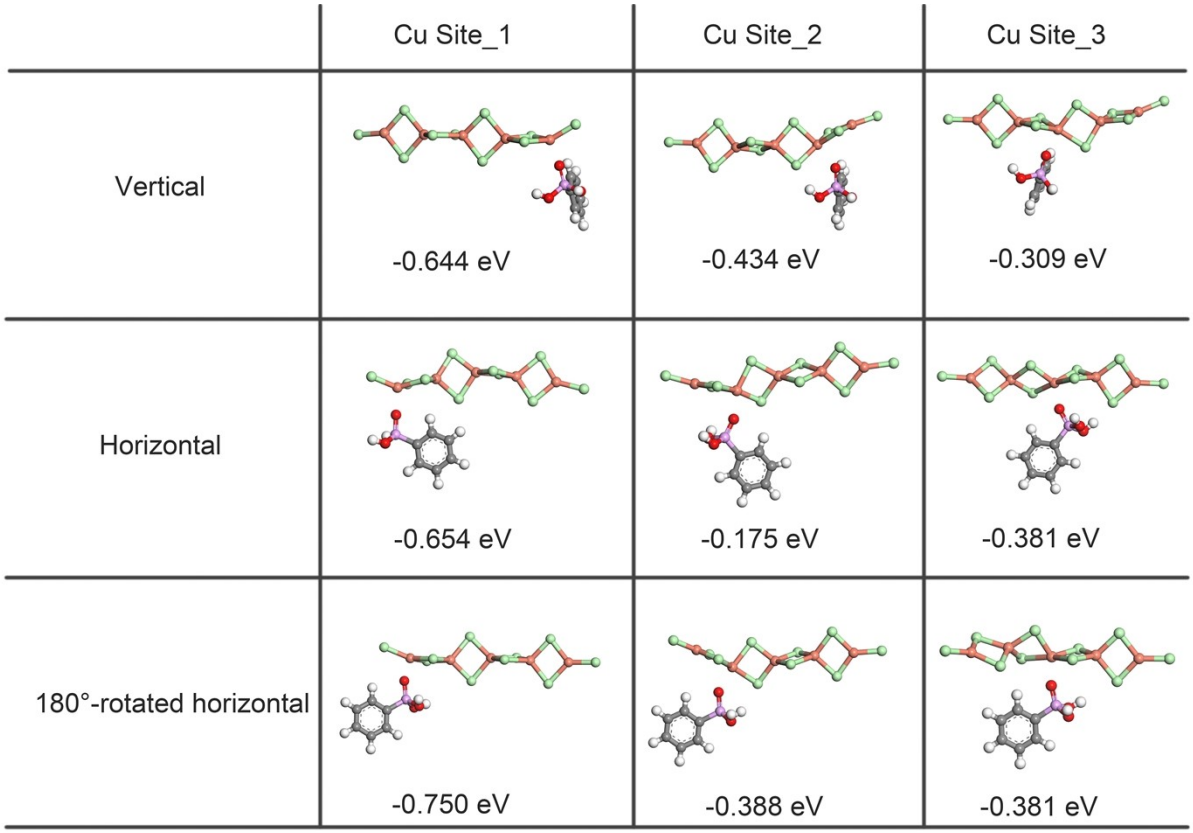

Figure S4. Different configurations of $CuCl_x$-PPA species. (The formation energy is listed beneath the corresponding structure)

	Cu Site_1	Cu Site_2	Cu Site_3
Vertical	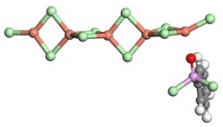 -0.383 eV	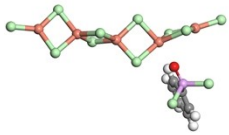 -0.123 eV	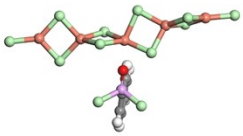 -0.116 eV
Horizontal	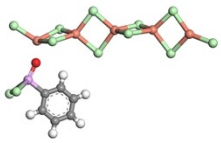 -0.445 eV	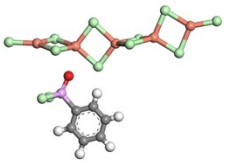 -0.240 eV	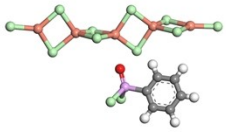 -0.205 eV
180°-rotated horizontal	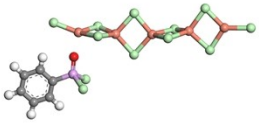 -0.393 eV	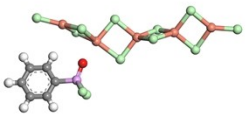 -0.102 eV	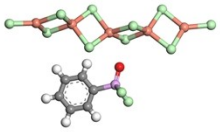 -0.256 eV

Figure S5. Different configurations of $CuCl_x$-BPDC species. (The formation energy is listed beneath the corresponding structure)

	Cu Site_1	Cu Site_2	Cu Site_3
Vertical	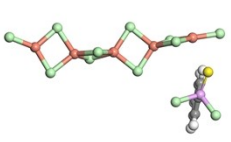 -0.310 eV	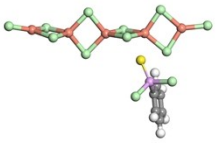 -0.056 eV	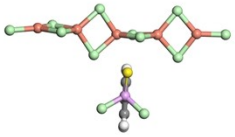 -0.117 eV
Horizontal	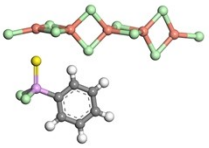 -0.383 eV	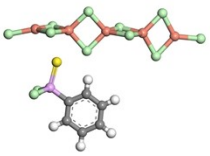 -0.246 eV	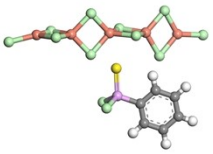 -0.128 eV
180°-rotated horizontal	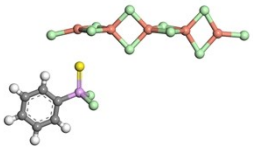 -0.352 eV	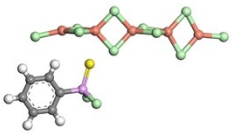 -0.014 eV	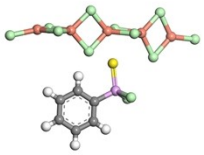 -0.013 eV

Figure S6. Different configurations of $CuCl_x$-PTDC species. (The formation energy is listed beneath the corresponding structure)

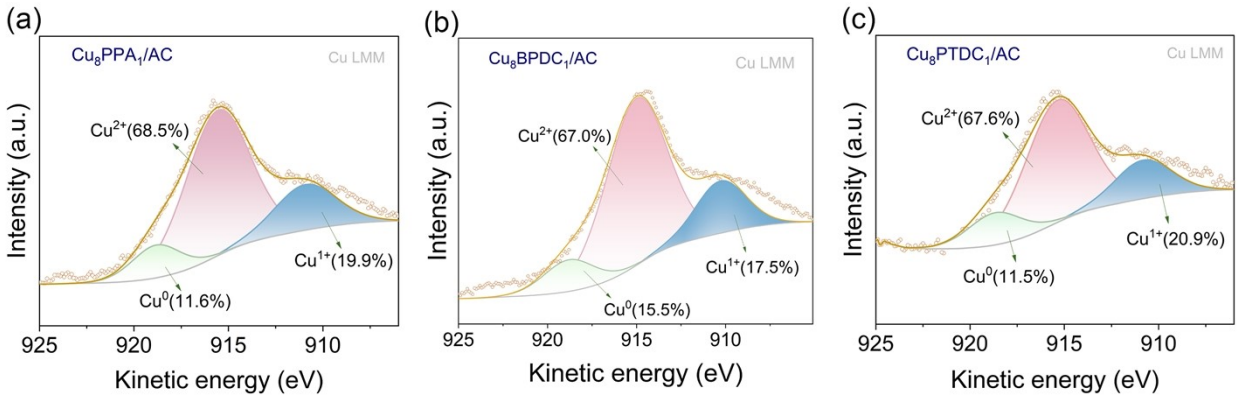

Figure S7. Cu LMM spectra of the (a) Cu_8PPA_1/AC; (b) Cu_8BPDC_1/AC and (c) Cu_8PTDC_1/AC.

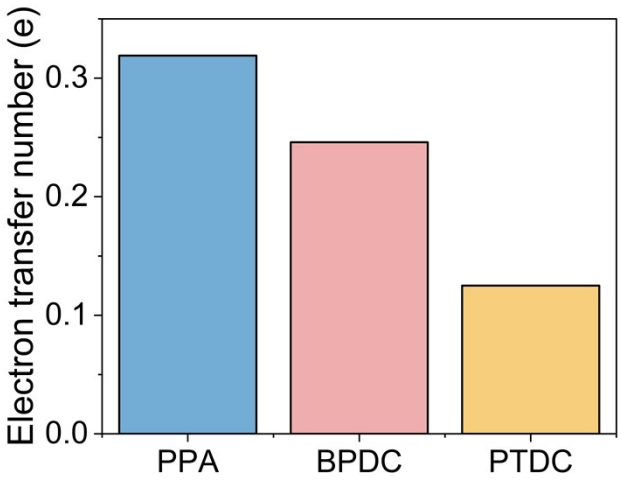

Figure S8. Electron transfer number for three $CuCl_x$-ligand systems.

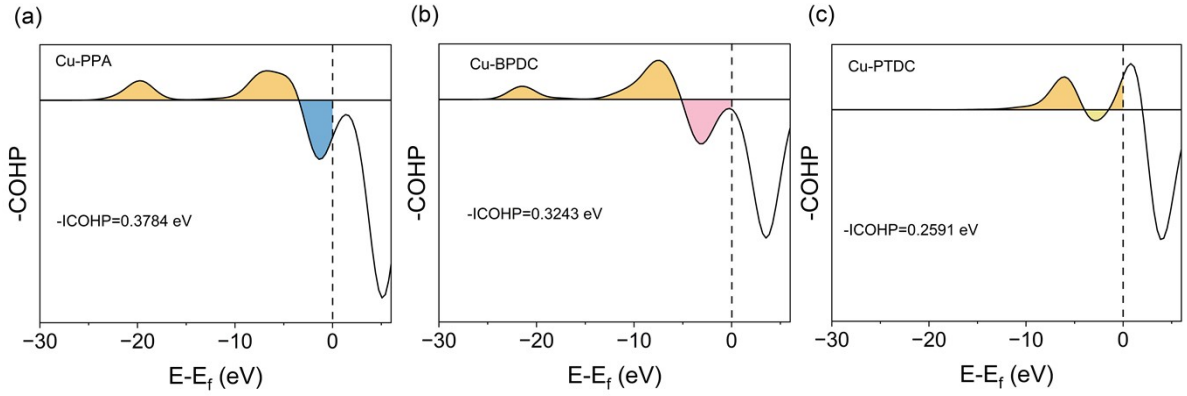

Figure S9. COHP analysis for three $CuCl_x$-ligand systems.

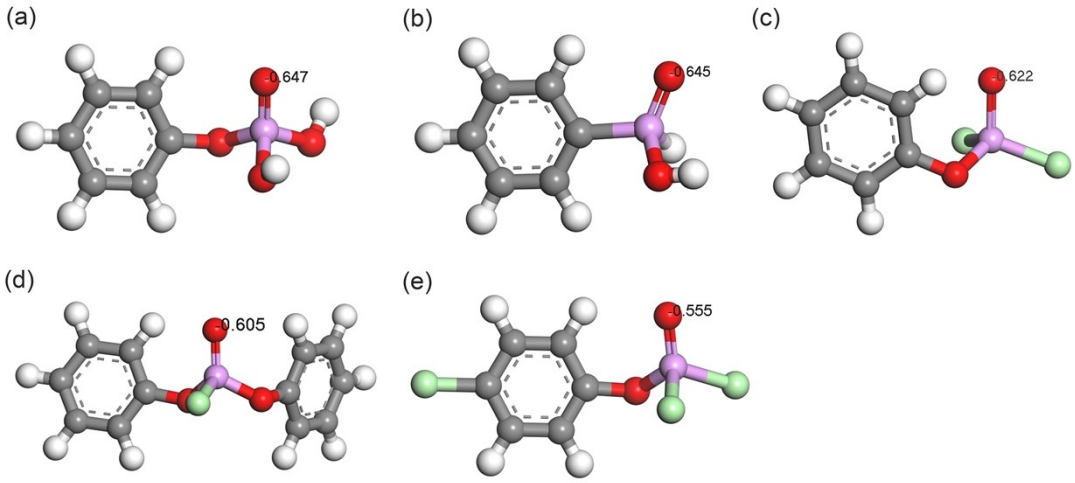

Figure S10. The Mulliken charge of the different atoms in the ligand about (a) PDPH; (b) PHPA; (c) PPDC; (d) DPCP; (e) 4-CPDP.

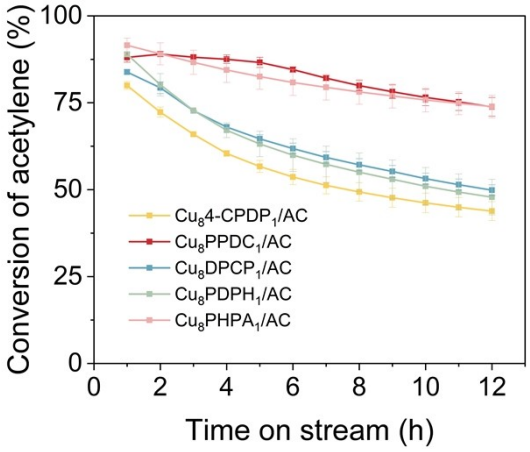

Figure S11. Catalytic performances of additional ligands. Reaction conditions: T = 180 °C, GHSV(C_2H_2) = 180 h^{-1} and V_{HCl}/V_{C2H2} = 1.15.

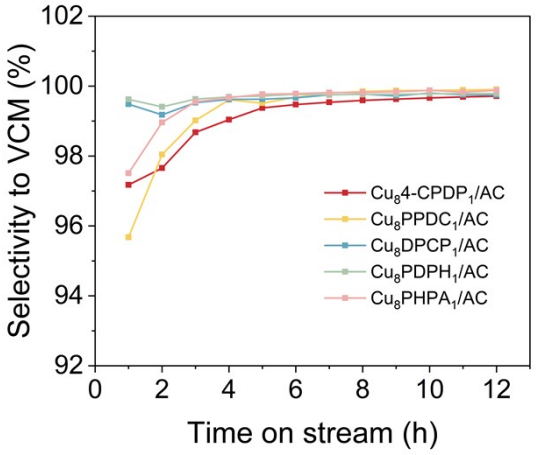

Figure S12. Catalytic selectivity to VCM of additional ligands. Reaction conditions: T = 180 °C, GHSV(C_2H_2) = 180 h^{-1} and V_{HCl}/V_{C2H2} = 1.15.

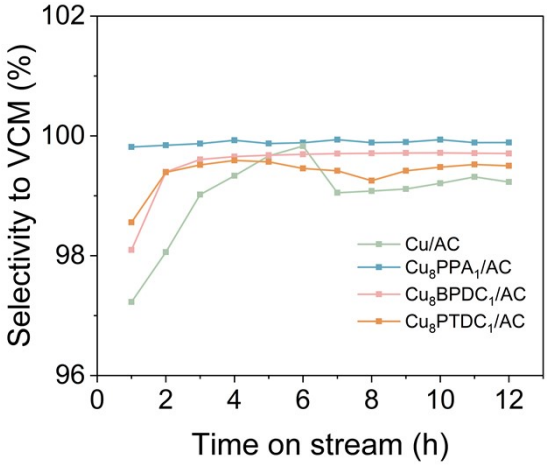

Figure S13. Catalytic selectivity to VCM of Cu/AC; Cu_8PPA_1/AC; Cu_8BPDC_1/AC; Cu_8PTDC_1/AC. Conditions: T = 180 °C, GHSV(C2H2) = 180 h^{-1} and V_{HCl}/V_{C2H2} = 1.15.

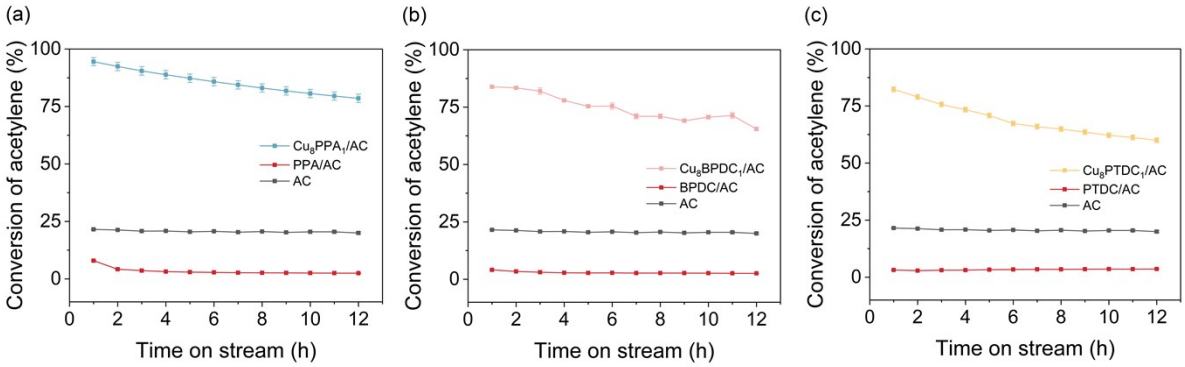

Figure S14. Catalyst performance evaluation of (a) Cu_8PPA_1/AC, PPA/AC and AC; (b) Cu_8BPDC_1/AC, BPDC/AC and AC; (c) Cu_8PTDC_1/AC, PTDC/AC and AC. Conditions: T = 180 °C, GHSV(C2H2) = 180 h^{-1} and V_{HCl}/V_{C2H2} = 1.15.

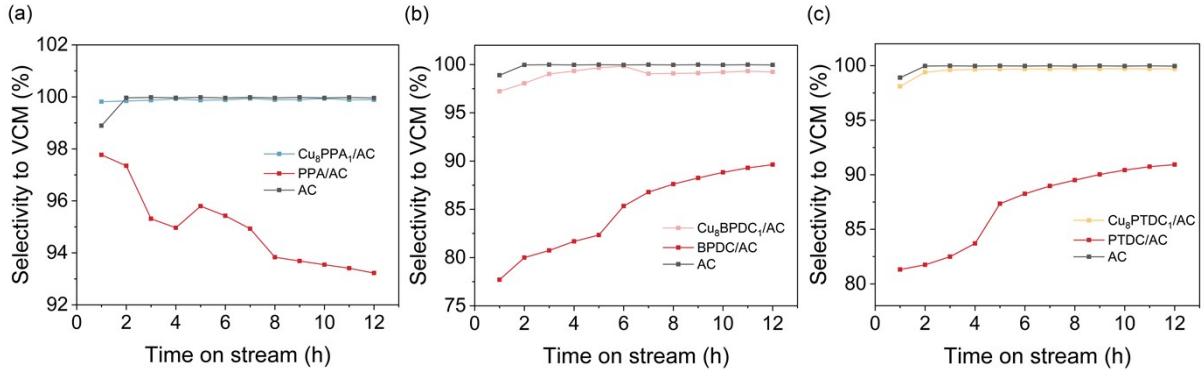

Figure S15. Catalytic selectivity to VCM of (a) Cu_8PPA_1/AC, PPA/AC and AC; (b) Cu_8BPDC_1/AC, BPDC/AC and AC; (c) Cu_8PTDC_1/AC, PTDC/AC and AC. Conditions: T = 180 °C, GHSV(C2H2) = 180 h^{-1} and V_{HCl}/V_{C2H2}=1.15.

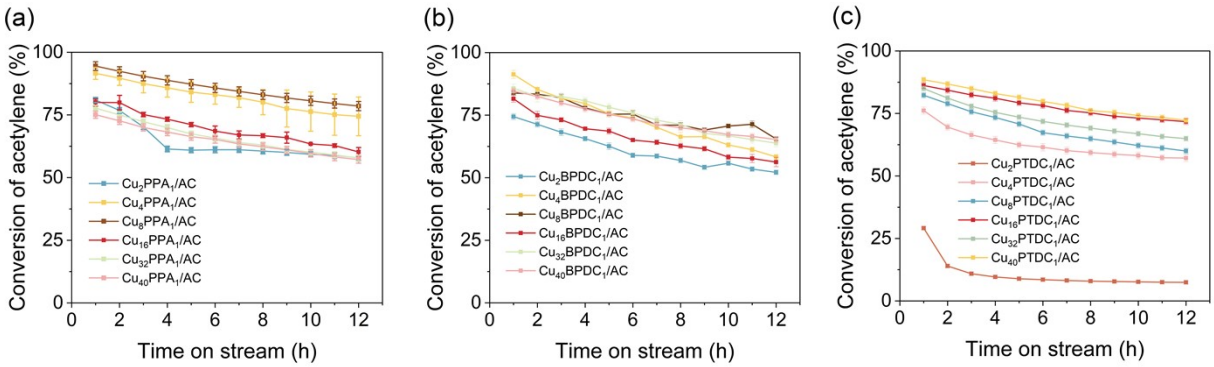

Figure S16. Catalyst performance evaluation of catalysts with varying ligand-to-metal molar ratios. Conditions: T = 180 °C, GHSV(C2H2) = 180 h^{-1} and V_{HCl}/V_{C2H2} = 1.15.

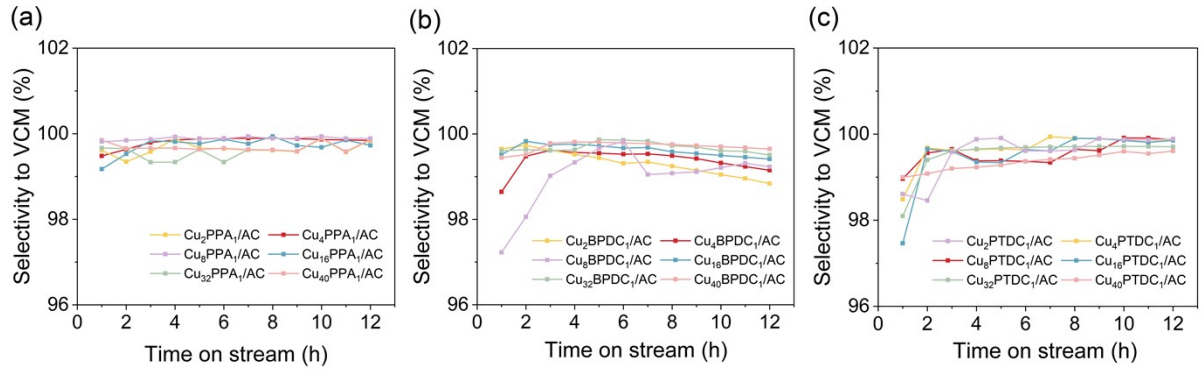

Figure S17. The selectivity to VCM of catalysts with varying ligand-to-metal molar ratios. Conditions: T = 180 °C, GHSV(C2H2) = 180 h^{-1} and V_{HCl}/V_{C2H2} = 1.15.

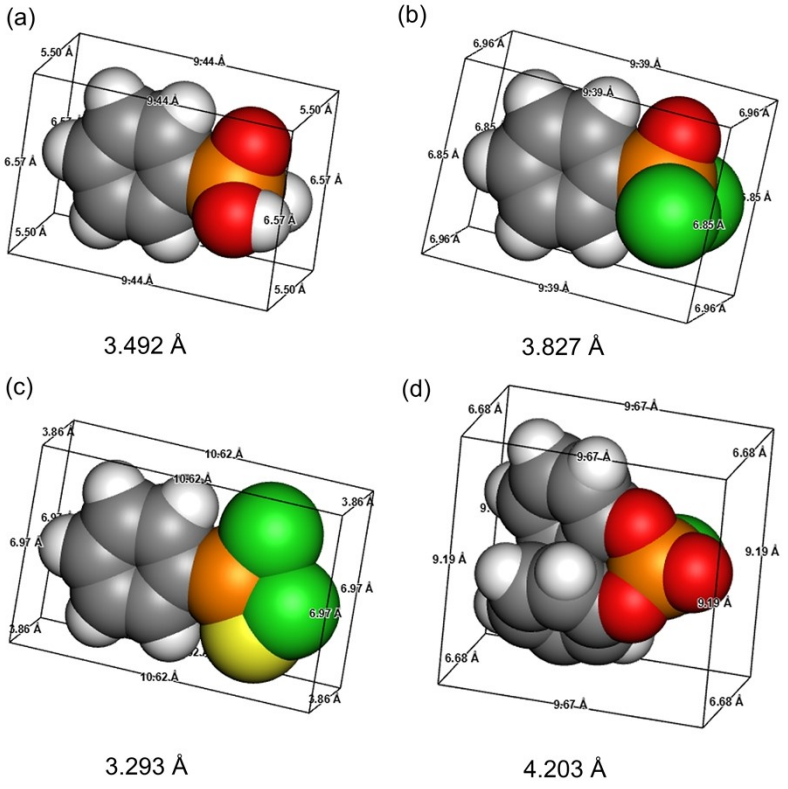

Figure S18. The molecular size of different ligands about (a) PPA; (b) BPDC; (c) PTDC; (d) DPCP.

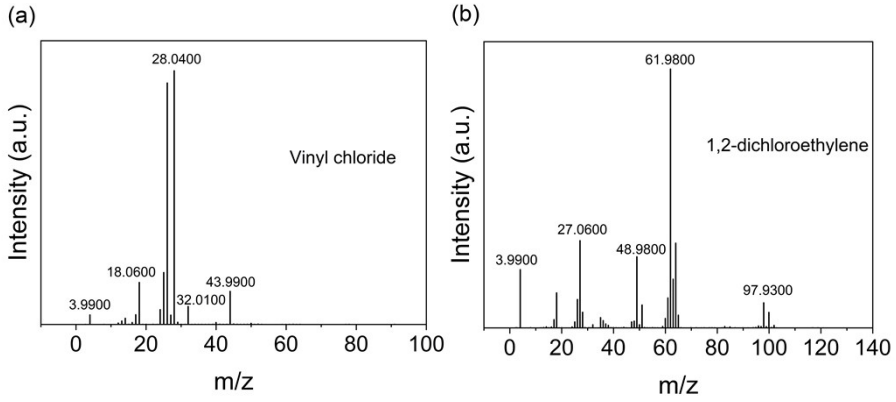

Figure S19. Mass spectrometry diagram about (a) Vinyl chloride; (b) 1,2-dichloroethylene.

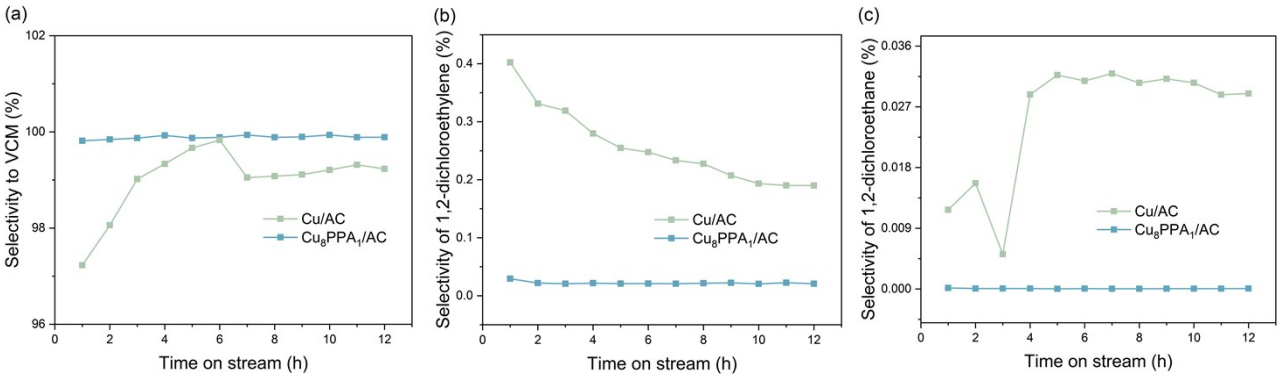

Figure S20. The selectivity to (a) VCM, (b) 1,2-dichloroethylene, and (c) 1,2-dichloroethane in the system Cu_8PPA_1/AC and Cu/AC. Conditions: T = 180 °C, GHSV(C2H2) = 180 h^{-1} and V_{HCl}/V_{C2H2} = 1.15.

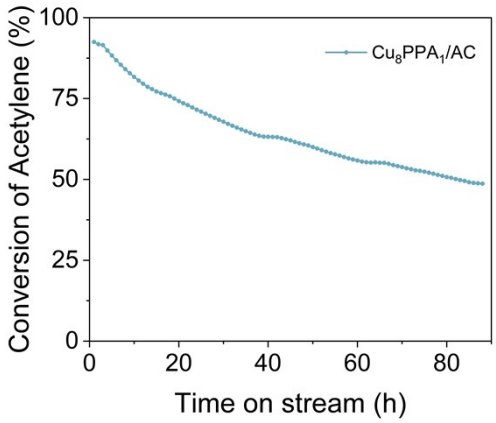

Figure S21. Evaluation of the long-term stability of the Cu_8PPA_1/AC catalyst. Conditions: T = 180 °C, GHSV(C2H2) = 180 h^{-1} and V_{HCl}/V_{C2H2} = 1.15.

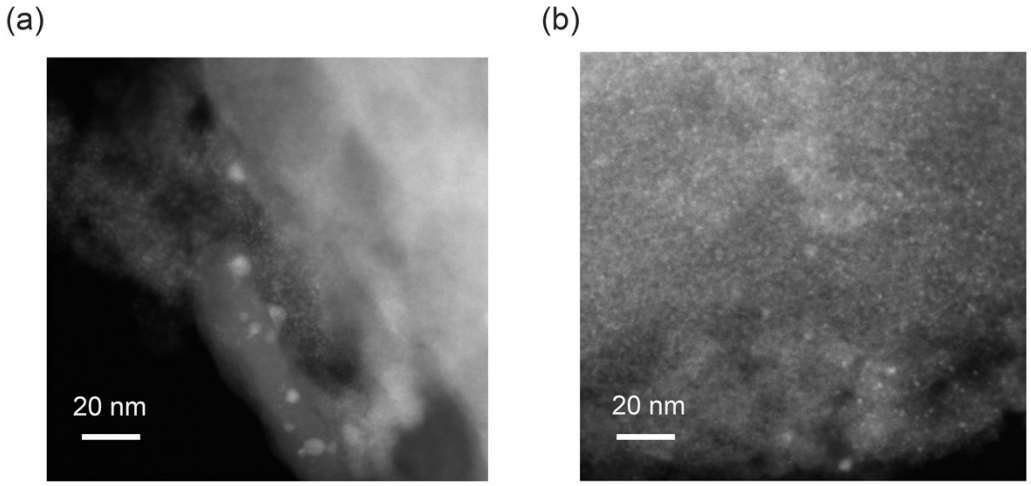

Figure S22. TEM images of (a) Cu/AC and (b) Cu_8PPA_1/AC.

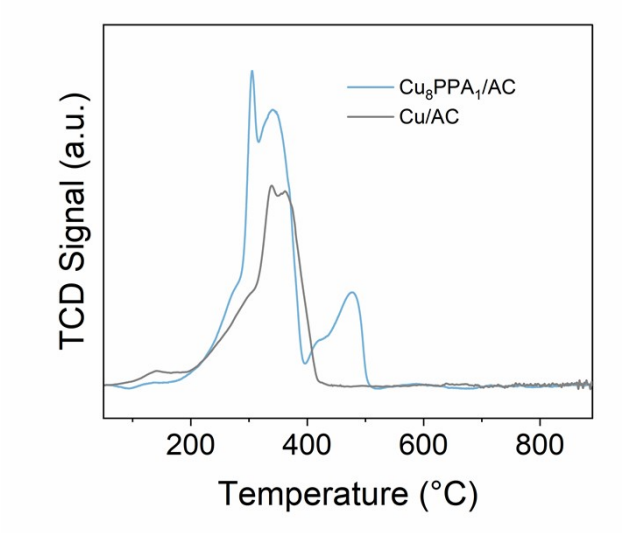

Figure S23. H_2-TPR profiles of Cu_8PPA_1/AC and Cu/AC.

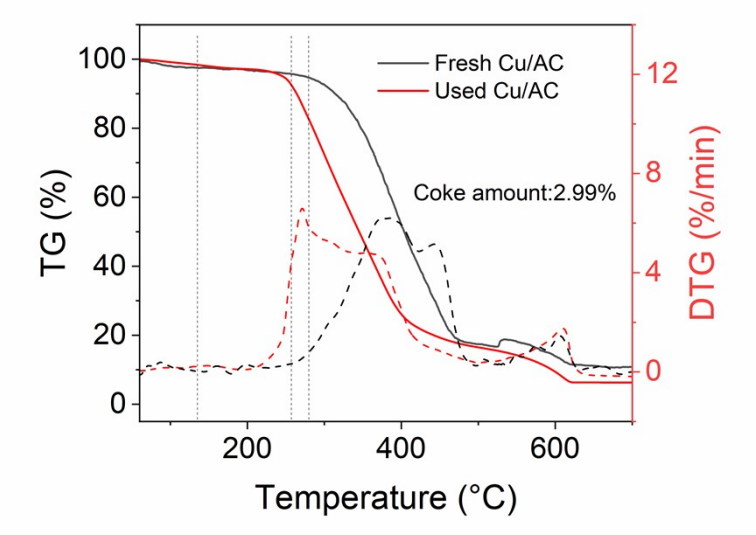

Figure S24. TG and DTG curves of Cu/AC.

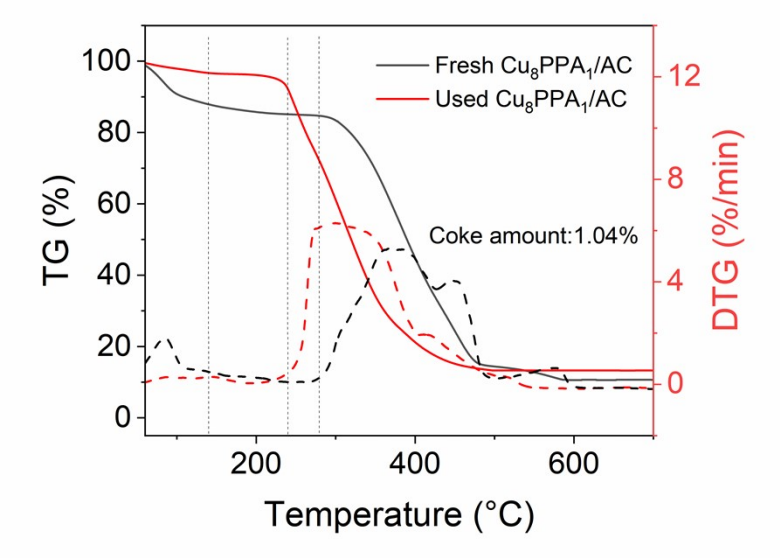

Figure S25. TG and DTG curves of Cu_8PPA_1/AC.

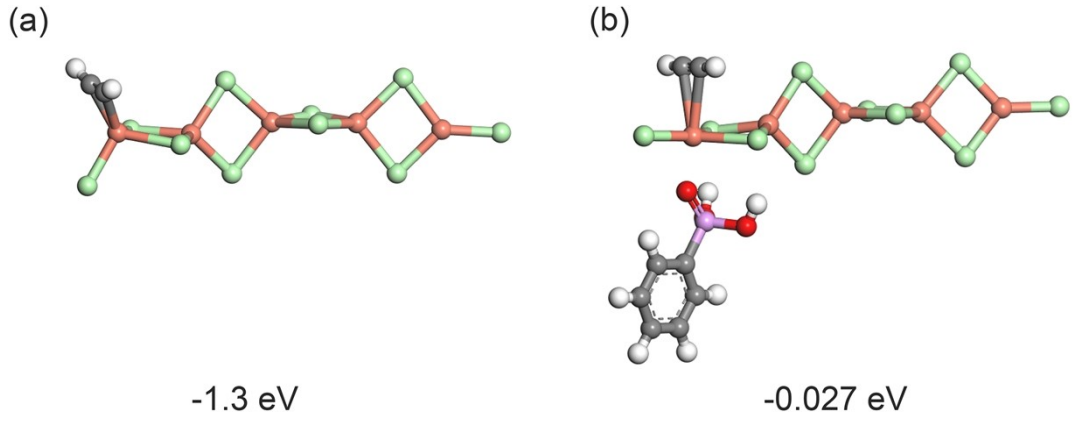

Figure S26. Adsorption models about (a) copper clusters and acetylene; (b) $CuCl_x$-PPA system and acetylene. (The adsorption energy is listed beneath the corresponding structure)

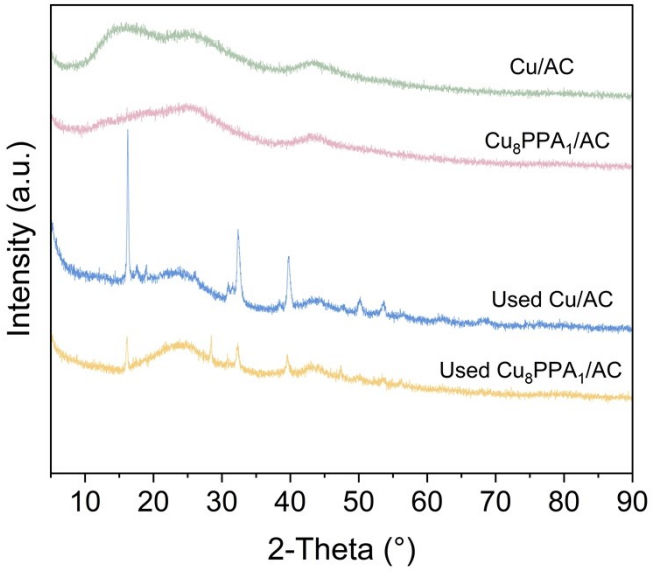

Figure S27. XRD patterns of Cu-based catalysts.

Table S1. The content of copper species in the catalyst based on the Cu LMM region.

Catalysts	Cu species (%)			Kinetic energy (eV)		
	Cu^{2+}	Cu^{+}	Cu^{0}	Cu^{2+}	Cu^{+}	Cu^{0}
Cu_8PPA_1/AC	68.5	19.9	11.6	915.57	910.92	918.82
Cu_8BPDC_1/AC	67.0	17.5	15.5	915.46	910.79	918.80
Cu_8PTDC_1/AC	67.6	20.9	11.5	915.37	910.82	918.67

Table S2. The adsorption capacity of different catalysts for HCl and C_2H_2 based on TPD curve.

Catalysts	The adsorption area for HCl			The adsorption area for C_2H_2		
	2:1	8:1	40:1	2:1	8:1	40:1
Cu/AC		100%			100%	
Cu-PPA	388%	189%	247%	70%	68%	75%
Cu-BPDC	246%	117%	147%	111%	63%	58%
Cu-PTDC	330%	328%	367%	99%	58%	63%

Note: The integrated area of the TPD profile for the reference Cu catalyst was defined as 100%, and the areas of all other catalysts were normalized accordingly.

Reference

[1] J. P. Perdew, K. Burke and M. Ernzerhof, *Phys. Rev. Lett.,* 1998, **80,** 891-891.

[2] Y. Wang, Y. Nian, J. L. Zhang, W. Li and Y. Han, *Mol. Catal.,* 2019, **479,** 55-65.